Scientific Research Publishing

American Journal of Analytical Chemistry, 2023, 14, 493-518
https://www.scirp.org/journal/ajac
ISSN Online: 2156-8278
ISSN Print: 2156-8251

Green Chemistry Allometry Test of Microwave-Assisted Synthesis of Transition Metal Nanostructures

Victor J. Law*, Denis P. Dowling

School of Mechanical and Materials Engineering, University College Dublin, Dublin, Ireland
Email: *viclaw66@gmail.com

How to cite this paper: Law, V.J. and Dowling, D.P. (2023) Green Chemistry Allometry Test of Microwave-Assisted Synthesis of Transition Metal Nanostructures. *American Journal of Analytical Chemistry*, **14**, 493-518.
https://doi.org/10.4236/ajac.2023.1411029

Received: October 27, 2023
Accepted: November 26, 2023
Published: November 29, 2023

Abstract

Microwave irradiation is considered an important approach to Green Chemistry, because of its ability to rapidly increase the internal temperature of polar-organic compounds that lead to synthesis times of minutes rather than hours when compared to conventional thermal heating. This works describes a dual allometry test for the discrimination between the solvents and reagents used in the microwave-assisted synthesis of transition metal (zinc oxide, palladium silver, platinum, and gold) nanostructures. The test is performed in log-log process energy phase-space projection, where the synthesis data (kJ against kJ·mol^{-1}) has a power-law signature. The test is shown to discriminate between recommended Green Chemistry, problematic Green Chemistry, and Green Chemistry hazardous solvents. Typically, recommended Green chemistry exhibits a broad *y*-axes distribution within an upper exponent = 1 and lower exponent = 0.5. Problematic Green Chemistry exhibits a *y*-axes narrower distribution with an upper exponent = 0.94 and lower exponent = 0.64. Non-Green Chemistry hazardous data exhibits a further narrowing of the *y*-axes distribution within upper exponent = 0.87 and lower exponent = 0.66. In all three cases, the *y*-axes is aligned to original database power-law signature. It is also shown that in the *x*-axes direction (process energy budget) the grouped order of magnitude decreases from four orders for recommended Green Chemistry solvent and reagent data, through two orders for non-Green Chemistry hazardous material and down to one order for problematic Green Chemistry.

Keywords

Microwave-Assisted Synthesis, Transition Metals Nanostructures, Allometry Scaling, Power-Law Signature, Green Chemistry

1. Introduction

The efficient use of the Earth's resources and production of less environmentally toxic waste has become codified in to the current twelve principles of Green Chemistry (Anastas and Eghbali 2010) [1]. In the case of microwave synthesis of metal nanostructures, organic polar and non-polar solvents, reagents, plant extract and bacteria extracts are becoming the Green Chemistry solvents and reagents of choice (Bharadwaj *et al.* 2021) [2], Joudeh and Linke (2022) [3], and Grewal *et al.* (2013) [4]. The twelve principles of this Green approach may be summarized as: 1) To prevent waste, rather than clean it up. Producing any material without realizable value can be regarded as waste. 2) Atom economy, that is the maximizing the use of material in the final targeted product. 3) Use environmental benign solvents, and generate less hazardous/toxic chemicals. 4) The use of solvents should be based on process safety, worker safety, environmental safety, and sustainability. 5) Chemical products should be designed for desired function while minimizing toxicity. 6) Design energy efficiency processes by exploiting every kJ of energy. 7) Use raw material rather than depleting whenever practicable. 8) Remove unnecessary derivatization, such as temporary blocking, capping, or modification should be avoided if possible. 9) Use catalytic reagents rather than stoichiometric reagents. 10) Chemical products should be designed so that at the end of their function they should be easily broken down without causing any danger to the environment. 11) Development of green analytical procedures for off-line and on-line process monitoring and control with the aim of producing less waste. 12) Design chemical processes using risking assessment to identify hazards, then design-out, or minimize hazards and accidents. The advantage of using microwave irradiation is that it selectively heats the reactant suspension as compared to thermal heating where the reaction vessel and surrounding apparatus is heated. Thereby reducing energy consumption, process time along with an increase in product yield. Although limited to a few grams in batch processing scaling-out through process intensification (minimization of reactor size, conversion from batch to continuous flow and appropriate solvent choice) is of growing interest and importance. The premise of this work is that the Green approach embodied within microwave synthesis is not based solely on its rapid processing time, but also on the chemicals used in the synthesis, or all twelve principles.

Recently historical data pertaining to microwave oven (operated in the batch processing mode) inactivation of bacteria or virus on different-fomites as been studied (Law and Denis (2022) [5]), and experimental reconstruction of their non-thermal microwave induced $\geq 4\log_{10}$ reduction in inactivation has been shown to be influenced by the experiential method and measurement (Law and Denis (2023) [6]). In these papers, a log-linear energy phase-space projection was used; where the process energy budget (cavity-magnetron power multiplied by process time ($J{\cdot}s^{-1} \times s = kJ$) is plotted on the x-axes and the process energy density (process energy budget divided by suspension volume, measured in ml, ($kJ{\cdot}mol^{-1}$).

Using the same energy phase-space projection technique, but using a log-log transformation of both *x*-axes and *y*-axes, historical microwave-assisted synthesis of transition metal nanostructures (monometallic, bimetallic structures, and metal decorated sheets) has also been examined: for silver (Ag), and gold (Au) (Law and Denis (2023) [7]), and for palladium (Pd), Ag, platinum (Pt), Au, and zinc oxide (ZnO) (Law and Denis (2023) [8]). Typically the synthesis operated within a multimode cavity the microwave power source operated at a free running frequency of f_o = 2.45 ± 0.05 GHz (free wavelength, λ ~ 12.2 cm).

In the case of the reconstruction experiments of non-thermal microwave-assisted inactivation of bacteria and virus revealed that microorganism resilience to microwave stress maps to iso-volume trend-lines, where the microorganism resilience increased from vegetative Gram-negative to vegetative Gram-positive and on to Gram-positive spores. MS2 and influenza viruses were also found to have an intermediate resilience dependency. Here the high dimensional-space of the process energy phase-space projection makes this information readily available. In addition, the dimensional-space reveals that both the original experimental and measurements techniques should be reconsidered as the cavity-magnetron duty-cycle conditions used significant influence the applied power measurement error within the microwave treatment time frame, typically 1 to 1.5 minutes [6]. Finally, combining the outcome for the Ag and Au (here referred to as Database A, n = 30) study [7], and the Pd, Ag, Pt, Au, ZnO (here referred to Database B, n = 50) study [8] a global power-law signature ($y = 0.7172x^{0.791}$, or an approximate 3/4 fraction is obtained. Using a log-linear plot of the linear regression residual data 3-sigma and non-parametric cluster, the power-law was verified over four orders of magnitude with outliers identified and associated with a microwave Digestion application-type and a phase-transition between microwave oven-type and microwave Digestion applicator-type. With regard to the physiochemical and microwave-assisted aspects of the power signature this still remains to be identified. In-line with the twelve principle of Green Chemistry, there is a need for an off-line non-linear test that is sensitive to Green chemistry solvents and reactants analytical test. Ideally applying a non-linear analytical test to historical microwave-assisted synthesis high-dimensional data within standard spread-sheet software will enable future waste products to be reduced.

It is the aim of this work to apply allometry (*Greek*: *alloios meaning different and metry meaning to measure [9]* [10]) to the microwave-assisted power-law signature generated within the energy phase-space projection, with focus on the individual transition metal (Pd, Ag, Pt, Au and ZnO) synthesis chemistries within Database B, n = 50. In this dataset forty-nine microwave applicators operate in the batch mode and one operates in the continuous-flow mode. The microwave applicators are: the domestic microwave oven, microwave ERTEC: model 02-02 (Wrocław-Poland) applicator, Temperature Controlled Microwave Chemistry (TCMC) applicators, and Digestion applicators.

Allometry analysis tools are established in the scientific field of biology, ento-

mology, and forestry and to our knowledge is not acknowledged as a metric in microwave-assisted processing analysis tool. In addition an allometry word search in the Scientific Research Publishing (https://www.scirp.org/journal/ajac/) did not find a hit in American journal analytical chemistry. Therefore section 2 provides a summary of allometry scaling terminology used in relative growth rate (RGR) studies, forestry studies and pharmacokinetics where a non-linear function is fitted to a non-linear distribution. Section 3 then describes how this metric may be transferred to microwave-assisted synthesis power-law signature that has a non-linear distribution when plotted in energy phase-space projection. The aim of these two sections is also to inspire readers of American Journal of analytical chemistry to use this analytical tool in new endeavors.

The remainder of this work is organized as follows. Section 4 presents the analytical approached used, including the reasons for employing non-thermal microwave-dielectric volume heating of water (H_2O) as a benchmark comparison. Section 5 examines the energy mapping parameters of each nanostructure data point as a response to the sum of mechanisms involved in the microwave-assisted synthesis. For example the third principle of Green Chemistry indicates that flammable and toxic regents and organic-metals (bromine (Br), potassium (K), and sodium (Na)) should be replaced with compounds that are benign to the environment. In the case of the seventh principle the use of raw material such as plant extract is the choice of use. Section 6 provides a summary and an outlook of this work.

2. Allometry, Geometry and the Quarter-Power Scaling Rule

In 1936, the biologist J.S. Huxley and the mathematician G. Teissier [9] [10] came together to coin the word "allometry" to unify confusing terminologies used when fitting an mathematical expression to physical support, RGR, and metabolic rate data accumulated from plants and animals (J. Gayon (2000) [11]). See for example; mammal bone weight to bone cross-sectional area scaling (G. Galilei (1638) [12]); growth and form (D.W. Thompson (1917) [13], heterogonic growth (A. Pézard (1918) [14]); relative growth (J.S. Huxley (1924) [15]); and dicharmonic growth (C. Champy (1924) [16]). In many of the early homoiothermrs (warm-blooded) mammal studies, the scaling exponent was considered to be governed by the surface-area-to-volume (sa/vol) measured in units of r^{-1}, where r is the radius of a sphere that represents the mammal body. This Euclidean geometry model has a two dimensional surface area (sa) and a three dimensional internal volume (vol) that equals to the fraction 2/3. In this body of work it is assumed that a two-variable power-law function can be fitted to the accumulated data when plotted on log-log graph format. Huxley and Teissier's two variable power-law takes on the form of Equation (1).

$$y = bx^{\alpha} \tag{1}$$

where: y is the differently growing body part of interest, x is the body size, b is y-axes intercept constant, and a is the exponent that defines the type of scaling

relationship between y and x. It is noted, that when $a < 1$ this will relate to a slow rate of growth (negative, or, *hypoallomerty*); an exponent = 1 would mean that the relationship is linear (or *isometry*); and if the exponent > 1 the growth rate is rapid (positive, or *hyperallometry*), as befits the early growth repose curve. [*N.B. for non physiology studies* (*bibliometric and city size*) *it is postulated that an exponent* > 1 *is the result of a positive feedback mechanism between input and outputs*, Dong (2017) [17]. The simple Euclidean geometry argument however does not address the fact that at the unicellular level (0.5 to 10 micrometers) plants and animals have a flexible membrane or cytoskeleton that can change shape (typically into a prolate cylinder, or rod) as that additional cylinder grows in axial length (L). As the spheroid elongates in one axis, the cylinder curved surface area ($S = 2\pi rL$) and cylinder volume ($V = \pi r^2 L$,) alters the cells morphology, and changes the cell sa/vol. For example a prolate cylinder of $L = r$, $L = 2r$ and $L = 3r$ the sa/vol becomes: 0.5, 0.48 and 0.61, respectively. Thus as an organism grows its volume increases at a faster rate than the outer membrane energy exchange surface. This argument also extends to the nanometer scale. For cube and pyramid structures, which have 6 and 8 linear edges respectively, sa/vol increases from 1.2 and 1.94. For flower-like structures that have acute angled spikes, sa/vol becomes very large for a given volume when compared to a solid sphere.

Biologist have found it useful to subdivide allometry scaling into a three related x and y relationships or, modes: Ontogenetic, static, and evolutionary allometry. Ontogenetic allometry refers to a RGR trait at given developmental stage of signal organism, static allometry measures the RGR trait among individuals at a similar developmental stage, and evolutionary allometry measures the RGR trait within populations or species. However, applying the two-variable power-law fit to ontogenetic and static studies introduces a problem in the RGR calculation as the two-variables may not be independent from each other, even though the relative slope is constant (Lamont, Williams and He (2023) [18]). This is generally not the case when the starting mass is a constant when compared to different organisms in the evolution mode. See for example, the temperate climate aerobic mouse-to-cow curve produced by Kleiber (1932) [19], and Kleiber (1947) [20] where the exponent equates to 3/4. This exponent has been found to be near universal and has become known as "Kleiber's Law" on metabolic scaling [21].

Today the general power-law function takes on different letters for the constant and exponent, depending on the scientific field of study (biology, chemistry, and physics), but in all cases it is used to mathematically describe the straighten properties of a curve when it undergoes a graphed log-log transformation. From a statistical analysis point of view, a reliable verification of a power-law function is only considered when the fit is over 1.5 orders of magnitude or more, on both the x-axes and y-axes [18], Rau (2002) [22], Stumpf and Porter (2012) [23], Andriani and McKelvey (2019) [24], and Roman and Bertolotti

(2022) [25]).

In 1997, G.B. West, J.H. Brown and B. Enquist (known here as WBE) put forward the theory of the fractal-like nature of internal resource-transport structure of biological systems [26], and more specific to vascular plants in 1999 [27]. Their theory is based on three principles.

Firstly, the network supplies the entire volume of the organism; a space-filling fractal-like branching pattern, where the total cross-section area of branching the network is preserved. *i.e.*, the sum of the cross-sectional areas of the daughter branches equals that of the parent (sum of daughter πr^2 = parent πr^2). Secondly, the final branch of the network (such as the capillary in the circulatory system) is a size-invariant unit. Thirdly, the energy required to distribute resources is minimized as there no hydrodynamic resistance within the system.

The allometry scaling therefore is governed by the physical and geometric constraints of these three principles which is a simple representation of a complex distribution network. In establishing their theory they acknowledged Jean of Jean Louis Marie Poiseuille (1799-1869) who developed the well known equation of volume transport per unit time (q), in a streamline flow through a cylinder, Equation (2) [21] [22] [28] and [29],

$$q = \left(p/8\right) r^4 P \big/ hL \tag{2}$$

where r is the radius, L the length of the cylinder, P the pressure drop across it, and h the viscosity of the fluid. Using this geometric theory, each daughter branch of the distribution system has half the length, one-eighth the cross-sectional area, and one-sixteenth the volume of the parent branch. In this way the WBE theory yields an exponent = 3/4. A further development of the WBE theory has been the addition of size and temperature thereby evaluating the resting metabolic rate to the maximal aerobic activity of an organism (Gillooly *et al.* (2001) [30], Downs, Hayes and Tracy (2008) [31]).

The world of pharmacokinetics has greatly befitted from the application of allometry. For example; Dedrick, Bischolt and Zaharko (1970) [32], Boxenham (1981) [33], and Boxenhan and Fertig (1984) [34] has shown that a mammals physiology is synonymous with pharmacokinetics time (gauged by the tempo of changes in a living organism, rather than chronological time) and maybe used to calculate interspecies total body drug clearance value expressed in unit of volume per unit physical time per body weight. This is based on the following observations:

Firstly, most mammals have four heartbeats per breath and have the same number of berths per lifetime, where small mammals have rapid heartbeat and short lifetimes, while larger mammals slow heartbeats and long lifetimes. Secondly, small mammals generally clear drugs from their bodies more rapidly in chronologic time per unit body weight than larger long-lived animals. But when measured individual physiological time, mammals tend to clear a drug at a similar pace. Thirdly, small mammals have relatively larger drug eliminating organs

such as liver and kidneys than do larger mammals. And because blood perfusion rates to these organs are roughly proportional to their sizes, small animals have a greater drug clearance (CL_{vivo}) measured in units of $ml \cdot min^{-1} \cdot kg^{-1}$ body weight.

Thus comparing a 0.022 kg mouse with a 70 kg human with the drug methotrexate CL_{vivo} which has a allometry exponent = 1/4, or 0.25 in decimal units. This yields a ratio 0.022 $kg^{0.25}$ (0.38) to 70 $kg^{0.25}$ (2.89) which approximates to 0.13:1. Boxenham [33] states this in pharmacokinetic terms of "*the mouse will clear the same volume of drug per kg body weight in* 0.13 *minutes as the human does in* 1 *minute*." For further reading on this subject, see Gilibili *et al.* (2015) [35].

3. Allometry Transfer to Microwave-Assisted Synthesis Energy Phase-Space Projection

From the knowledge presented in Section 2, it is the assertion here that the terminology and the two-variable power-law function scaling used in allometry studies (size and shape, mammal metabolic rate studies, and pharmacokinetics) may be transferred with confidence to microwave-assisted synthesis of nanostructures. Furthermore as with Andresen, Shiner and Uehlinger (2002) [36], the question "does the empirical data provide a scaling law" is turned around to ask a does the empirical scaling law provide functional information? For example, does the process energy budget increase due to changes in dielectric properties of solvents and reagents and how much by? Does, suspension bulk temperature (T_B) govern by the process energy budget, where T_B << the dielectric volume heating the instantaneous temperature (T_i).

What is known that from an energy phase-space projection point of view is that the variation in microwave applicator-type and the variation in mammal species have a finite and bounded space that can be mapped throughout the projection with their class traits distinguishing their coordinate position. For example microwave applicators (having a power source that operates at a $f_o = 2.45 \pm 0.05$ GHz ($\lambda \sim 12.2$ cm) have a specific dielectric volume heating trait that is absent in direct current, and radio frequency power source applicators. Thus a microwave applicator-type when mapped in energy phase-space reveals it impact on the final synthesized product [5] [7] and [8]. This is similar to how Kleiber's showed the basal metabolic rate of the mouse-to-cow curve, equals their body mass raised to the 3/4 power law [19] [20] and [21].

The term "physiological time" used in scaling of different organism [28] [36] and pharmacokinetics [32] [33] [34] [35] denotes a variable time-scale (heartbeat or respiration) among organisms that can be related to the power on-time (T_{on}) within a cavity-magnetron duty cycle, where T_{on} plus T_{off} equals the base-time, and T_{on} minus base-time equals to the duty cycle. Hence the accumulated cavity-magnetron power on time (T_{on} multiplied by the number of base-times used) as the time used in the process energy budget calculation that is presented on the x-axes of the energy phase-pace projection [5] [6] [7] [8]. This would

mean that clock-time (as seen by an outside observer) does not directly control the process energy budget. From suspension temperature point of view, T_i can be considered a constant in the accumulated time, but the T_B profile becomes desynchronized from the direction of process energy budget. Taken together with the work of [36] this would indicate that the energy phase-space projection provides minimum thermodynamic entropy (ΔH) and a maximum energy efficiency value for the solvents and reactants used in each of the individually mapped microwave-assisted synthesized processes.

4. Analysis Methodology

The aim of this section is to provide a structured overview of the approached to allometry scaling of microwave-assisted synthesis data within an energy phase-space projection.

4.1. High-Dimensional Data Spread Sheet Design

Microsoft Excel spread sheet software is used collate the microwave-assisted high-dimensional data then dimensionally reduce the data [37] for visualization as a XY scatter plot. Plot facets, shape and color are use to delineate the five microwave applicator-types, five metal precursors and the solvent and reagents used that comply with the principles of Green Chemistry. The XY scatter plots use log-log transformation and linear regression power function trend-line is then fitted to the data **Figure 1**. The trend-line is then modeled using the Excel power function (= POWER(A1, 2, 3, Y1)*Z2), where A1, 2, and 3 are the cell coordinates, and the cells Y1 and Z2 are the values of the c and n constants of Equation (1). This power function, generators a 0-dimensional (0-D) model identity-line that represents the process energy density prediction at each observed process energy budget value.

4.2. Allometry Scaling

To provide a quantitative guide that brackets (captures) the data over four orders of magnitude on both axes, two allometry boundaries are constructed. The upper boundary has a fixed *isometry* exponent of 4 × 1/4 = 1, and the lower boundary is initially set to a *hypoallomerty* exponent of 2 × 1/4 = 0.5. The upper and lower allometry boundary y-axes intercept are set to the original Database B trend-line y-axes intercept of 0.7837 kJ·mol^{-1}. The underlay assumption here is that there is only one intercept for Database B. Due to the five microwave applicator-type with the database this is a simplistic assumption. This may be considered as a good starting point as in reality the y-axes intercept does not exist due to the warm-up time of the cavity-magnetron which approximates to 3 s [6]. For a cavity-magnetron rated at 800 W operating in CW mode, the estimated process energy budget lower limit (x_{min}) equates to 800 W multiplied by 3 seconds = 2.4 kJ, see the right hand side of **Figure 1**.

Using the 0-D model predicted values, residual error (RE) is calculated from

X-Y scatter graph

Paper	Appliactor	Load	Energy (x-axis)	Energy density	Model n = 0.5	Model n = 0.764	Model n = 1	Residual error	Power constant	Power constant	Power constant
Law2023	MO	dummy load	291	29.1	13.4	59.8	228.1	-231.2	**0.5**	**0.764**	**1**
Law2023	MO	dummy load	1000	100	24.8	153.5	783.7	-846.5	**0.7837**	**0.7837**	**0.7837**
Law2023	MO	tube-in tube	1129	112.9	26.3						
Law2023	MO	beaker	1310	131	28.4						
Law2023	MO	beaker	1856	185.6	33.8						
Bayazit2016	Discover	Au-rods	3200	810	44.3						
Rademacher2022	Discover	Pd-shard	120000	600	271.5						
Liu2019	MO	Zn-flower	120000	2400	271.5						
Cao2004	MO	Zn-flower	126000	31500	278.2						
Li2011	MO	Zn-flower	180000	3150	332.5						
Cai2023	MO	Zn-flower	204000	887	354.0						
Cao2011	MO	Zn-flower	204000	2040	354.0						
Hasanpoor2015	MO	Zn-flower	380000	3800	483.1						
Aljaafari2020	MO	Zn-flower	216000	2160	364.2						
Elazab2018	MO	PdCuO	7500	348.8	67.9						
Nadagouda2007	MO	Au	16200	6000	99.7						
Yazmin2014	MO	Au(s)	21600	4725	115.2						
Nadagouda2017	MO	Au-PCH	21600	9000	115.2						
Bhosle2015	MO	Au-flower	30000	8727	135.7						
Shah2019	MO	Au-hex	37800	16000	152.4						
Jyohai2020	MO	Ag(s)	45000	480	166.2						

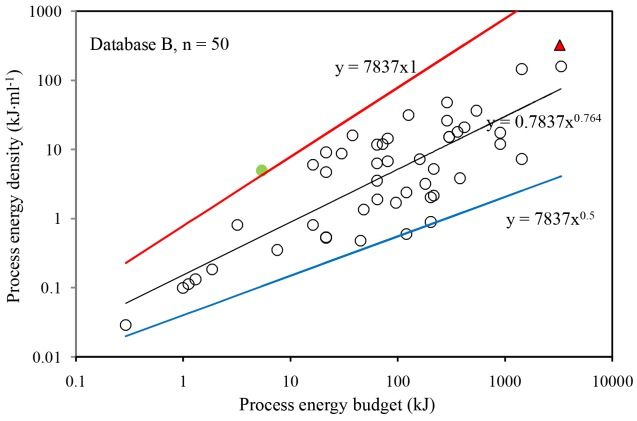

Figure 1. A section of the Excel spread-sheet showing a section of Database B collated microwave-assisted synthesis data for energy phase-space projection. To the right is a log-log energy phase-space projection for Database B, n = 50. Upper allometry boundary (thick red line with exponent 1), lower allometry boundary (blue line with exponent 0.5) and black is the linear regression trend-line with exponent 0.764.

the (P_v) minus the observed value (O_v), Equation (2).

$$RE = P_v - O_v \tag{2}$$

where the lower allometry boundary intercepts a given data point, *RE* is calculated as the difference between the 0-D model and the allometry intercept.

In **Figure 1** the first feature of note is that data regression trend-line forms a power-law signature over four orders of magnitude in both the *x*-axes and the *y*-axes. In addition the trend-line splits the data into 24 points above and 26 below the line. With a total ± data summation = 500 kJ·mol^{-1}. These two inequalities indicate the data points have a non-linear distribution [23] [24]. The second feature of note is that the upper allometry boundary exponent = 1 and lower allometry boundary exponent = 0.5 brackets (captures) 49 out of 50 data point, which equates to a 98% selectivity. The upper boundary outlier (green filled circle) has a residual error of +2.342 kJ·mol^{-1} which represents a one-pot Ag nanostructure synthesis employing Benzo-18-crown-6 ($C_{20}H_{24}O_6$) that acts both as reducing and stabilizing reagent within a Samsung CE2877 domestic microwave oven (Pal, Deb and Deshmukh (2014) [38]. For the same database, Law and Denis (2023) [8] used raked Residual error analysis and principle component analysis to shows that the Pt (3240 kJ, 324 kJ·mol^{-1} (Li *et al.* (2006) [39]) data point (red triangle) has a +3-Sigma outlier value, however this is not identified by the upper allomtery boundary: In this case an upper allometry exponent = 0.865 is required **Table 1**. These different outcomes are not incompatible as they are made in log-log space that has been transformed from and log-linear space. In log-linear space the emphasis is on outliers and where linear statistical mathematics such as 3-Sigma can operate. In log-log space the emphasis is on identifying a

function over orders of magnitudes where possible outliers far away from the origin (right-hand end of the curve) are compressed in the vertical scale to give a visually misleading illusion. Moreover, in the case of Figure 1, where the constant is kept close to zero, an exponent > 0.768 will eventually not capture any of the data points at the extreme end of *x*-axes. By extension using an upper and lower allometry boundaries, where their intercept constant are the same and the exponent varied between 0.5 and 1, all or no data points will bracketed or captured.

4.3. Non-Thermal Microwave Dielectric Volume Heating of H_2O as a Bench Mark Comparison

Process energy budget data for non-thermal microwave dielectric volume heating of H_2O at 2.45 GHz is used as a benchmark comparison [6] for the microwave-assisted synthesis of transition metals reported here. The reason being that H_2O is classed as moderate microwave energy absorber with a loss tangent ($\tan\delta_e = \varepsilon_r''/\varepsilon_r'$) of approximately 1.35˚C at 20˚C. The dielectric properties (real (ε_r') and imaginary (ε_r'') parts of its complex permittivity, and $\tan\delta_e$ are given Table 2 for the environmental temperature range of 20˚C to 25˚C and at a temperature of 100˚C (law and Denis (2001) [40]. For comparison the dielectric real and imaginary values for ethylene glycol $C_2H_4(OH)_2$ which have one relaxation peak in the 40˚C to 805˚C range is classed as a fast microwave energy absorber with $\tan\delta_e = 0.16$ at 100˚C (Rana and Rana (2014) [41] and Patil *et al.* (2012) [42]) are also given. This comparison shows the that $C_2H_4(OH)_2$ with its high boiling point and $\tan\delta_e$ will be more effective in absorbing microwave energy and consequently induce rapid heating at higher temperatures when compared to H_2O. This does not preclude other solvents from being used, however as it will be shown in section 5.1, H_2O is the primary solvent used in the microwave hydrothermal synthesis of ZnO nanostructures and is replaced by $C_2H_4(OH)_2$ in the microwave solvothermal synthesis of ZnO nanostructures.

Table 1. Residual error outlier parameters and allometry outlier test.

Outlier data point	Metal	x-axes (kJ)	y-axes (kJ·mol^{-1})	Residual error (kJ·mol^{-1})	Allometry Exponent
Samsung CE2877 [38]	Ag	5.40	4.909	+ 2.342	1.015
MARS-5 [39]	Pt	3240	324	+ 250	0.865

Table 2. Distilled H_2O and $C_2H_4(OH)_2$ real and imaginary complex permittivity, $\tan\delta_e$ at 2.45 GHz for an environmental temperature of 20˚C to 25˚C and temperature of 100˚C at one atmospheric pressure.

Solvent	Boil point (˚C)	ε_r' (20˚C to 25˚C)	ε_r'' (20˚C to 25˚C)	$\tan\delta_e$ $\varepsilon_r''/\varepsilon_r'$	ε_r' (100˚C)	ε_r'' (100˚C)	$\tan\delta_e$ ($\varepsilon_r''/\varepsilon_r'$)
H_2O (distilled)	100	~78	~12.5	~0.16	~80.4	~9.889	~0.045
C_2H_4 $(OH)_2$	197	~37	~49.95	~1.35	~25	~4	~0.16

4.4. Green Chemistry Catergory

The use of solvents has been a great environmental concern for the last few decades with many metric and selection guides published. Here we use a reduced form (three) of the six point guide formulated at (http://www.chem21.eu/) and [43]. The reason for this is to keep clarity in both dataset facets and plots. The reduced point guide is as follows: recommended, problematic and hazardous. Using this formulation H_2O, $C_2H_4(OH)_2$, bacteria extraction and plant extractions are in the Green Chemistry group, light molecular weight caustic compounds (potassium hydroxide (KOH), sodium hydroxide (NaOH), and sodium peroxide (Na_2O_2)) are in the problematic group. Finally organic-bromide and flammable hydrazine hydrate are in the hazardous group (Table 3).

5. Results

In this section, the energy phase-space projection of the microwave-assisted synthesized transition metals Pd, Ag, Pt, Au and ZnO nanostructures is mapped as a whole (Figure 1). For clarity the chemical is mapped to their associated modern periodic table groups, Group IV (ZnO) (Figure 2); Group V (Pd, Ag) (Figure 3); and group V (Pt, Au) (Figure 4).

5.1. Group IV: ZnO

Figure 2 shows the ten ZnO data points plotted in energy phase-space, the upper allometry boundary is kept at an exponent = 1 and the lower allometry boundary exponent is adjusted to 0.57 to intercept the lower $kJ \cdot mol^{-1}$ data point. The first feature of note is that the original Database B trend-line bisects the data points, 2 above and 8 below. Note, also that the ZnO data is tightly grouped in the *x*-axes (72 to 900 kJ) as compared to the four orders of magnitude for the whole dataset.

In the 0.7837 to 1 exponent region two microwave-assisted syntheses are located

Table 3. Short form of green chemistry solvents and reagents.

Recommended	Recommended or problematic	Problematic	Problematic or Hazardous	Hazardous	Highly hazardous
Green Chemistry		Problematic Green Chemistry		Non-Green Chemistry hazardous	
Water		Potassium hydroxide		Cetyltrimethyl ammonium bromide	
Bacterial extract		Sodium hydroxide		Hydrazine hydrate	
Acetic acid		Sodium peroxide			
Carboxymethyl-cellulose sodium		(3-mercaptopropyl)trimethoxysilane			
Dextrose, Glucose Maltose and Sucrose					
Dimethyl sulfoxide					
Ethanol					
Ethylene glycol					
Plant extracts					
Polyvinylpyrrolidone					

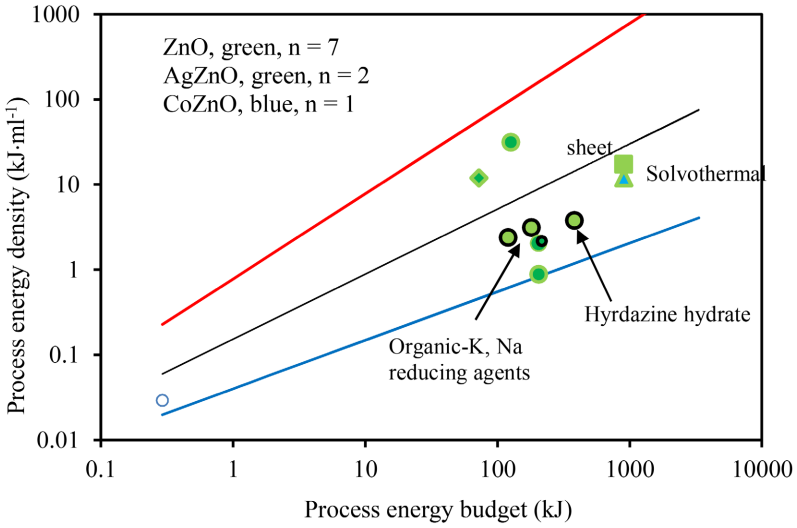

Figure 2. Log-log energy phase-space projection of nine ZnO and AgZnO (green), and one CoZnO (blue) nano-flower structures. Circle = Microwave oven applicator, square = TCMC applicator, diamond = ERTEC applicator, and triangle = Digestion applicator. Allometry scaling: red line = exponent of 1, blue trend-line = exponent of 0.57, and thin black line = original Database B trend-line with an exponent of 0.764.

in the 72 to 126 kJ process energy budget range. In this group Cao *et al.* (2004) [44]) employed a LG-MS-2079T microwave oven for the Green Chemistry synthesis of flower-like ZnO nanosheet aggregates (green circle). Also, Krishnapriya, Praneetha and Murugan (2016) [45] employed a Anton-Paar microwave Pro Digester for microwave-assisted hydrothermal process (using $(CH_3CO_2)_2Zn{\cdot}2H_2O$ + NH_3 in H_2O at a crystal formation temperature of T_B = 50˚C and a final process T_B = 125˚C with an autogeneous pressures up to 80 bar for the synthesis of ZnO jasmine-like nanostructures on sheets (green diamond). Here it is worth noting that NH_3 is used instead of $C_2H_4(OH)_2$.

In the exponent 0.57 to 0.7837 region six microwave ovens are located in the 120 to 380 kJ process energy budget range. These are: Cao *et al.* (2011) [46] used $C_2H_5NO_2$ and H_2O to reduce $(CH_3CO_2)_2Zn{\cdot}2H_2O$ to form flower-like nanostructures within a Galanz microwave oven (green filled circle). Li *et al.* (2011) [47] used NaOH, commonly called caustic soda or lye, to reduce $(CH_3CO_2)_2Zn{\cdot}2H_2O$ within an unspecified microwave applicator operating at 500 W with 50% duty cycle for the synthesis of ZnO and AgZnO flower-like nanostructures (green filled circle with black ring). Hasanpoor, Aliofkhazraei and Delavari (2015) [48] used a LG-MS1040SM microwave oven for microwave hydrothermal synthesis of ZnO flower-like structures. In their reaction toxic/farmable hydrazine hydrate is mixed with H_2O is used to reduce $(CH_3CO_2)_2Zn{\cdot}2H_2O$, but did not report a T_B value, and whether the reaction vessel was sealed, if so no autogeneous pressure is given (green filled circle with black ring). Liu *et al.* (2019) [49] used a unsealed reflux apparatus to heat a mixture of $AgNO_3$ and ZnO precursors plus $C_2H_4(OH)_2$ and Na_2O_2 within an unspecified microwave oven for microwave-assisted hydrothermal synthesis of Ag decorated flower-like ZnO nanosheets at

$T_B \sim 200^{\circ}C$. Here it can be assumed that the reflux apparatus exit aperture was at 1 bar atmospheric pressure (green filled circle with black ring). Aljaafari, Ahmed, Awada and Shaalan (2020) [50] used KOH, commonly called caustic potash to reduce $(CH_3CO_2)_2Zn{\cdot}2H_2O$ within an unspecified Samsung microwave oven (green filled circle with black ring). Finally, Cai and Hung (2023) [51] used a P70D10P-TE Galanz microwave oven to synthesis ZnO flower-like nanostructures (green circles).

Grouped to the right at a process energy budget of 900 kJ are two microwave syntheses. A TCMT applicator for synthesis of ZnO flower-like nanostructures (green square) (Li *et al.* (2014) [52]), and a ERTEC microwave applicator used for microwave solvothermal synthesis of Co doped ZnO compact "cauliflower" nanostructures (blue triangle) (Wojnarowicz *et al.* (2018) [53]).

Within the energy phase-space projection it can be seen that the visual comparison of recommended Green Chemistry synthesis (data points with green ring) with non-Green Chemistry synthesis ([47] [48] (black ring) can be made. Given this limited data, it may be generalized that organic-Br, K, and Na reagents are less efficient in terms of $kJ{\cdot}mol^{-1}$ than Green Chemistry alternatives. With regard to Green Chemistry solvents and/or reagent used in microwave-assisted synthesis, a more appropriate grouping would be [44] [45] [46] [51] [52] [53] and [54]. Reference [47] NaOH, [49] uses Na_2O_2 and [50] uses KOH, all of which are in problematic group.

Possible Ethylene Glycol Synthesis Reaction

The application of microwave irradiation as an energy source to process materials has become part of the Green Chemistry approach to chemical synthesis. This is mainly because of the reduced processing time required when compared to classical (thermal processing). Nevertheless chemicals that are flammable or harmful to the environment have been reported in microwave-assisted synthesis should be avoided in-line with the third and forth principles of Green Chemistry. It is worth noting that out of the ten ZnO nanostructure synthesis reported here, only four [44] [45] [49] and [52] directly use the words, clean, environment-friendly, green, or benign to characterize the their microwave technology. The microwave-assisted hydrothermal [45] [48] and [49] and solvothermal synthesis [53] claim to be part of Green Chemistry approached due to how organic reducing agents and solvents react in a compressed and high temperature environment. In this section the role in which H_2O and $C_2H_4(OH)_2$ are used to produce ZnO nanostructure is considered.

Combining the early work of Wojnarowicz *et al.* (2016) [54] with [53] and [49] provides three representative Equations (3)-(5) that illustrates how the contrasting dielectric properties of H_2O and $C_2H_4(OH)_2$ under different temperature and pressure conditions influence both the morphology and Co dopping of the ZnO nanostructure. In each case the remaining byproducts are classed as waste products.

Microwave hydrothermal within reflux apparatus within microwave oven [49]

$$\left(CH_3CO_2\right)_2 Zn \cdot 2H_2O + AgNO_3 \xrightarrow{C_2H_4(OH)_2, H_2O, Na_2O_2, \sim 200^\circ C} AgZnO + \text{waste products} \quad (3)$$

where AgZnO represents the overall reaction of Ag decorated ZnO nanosheets at $T_B \sim 200^\circ C$. Here 50 ml of H_2O, 1 mmol of $C_2H_4(OH)_2$ and 1 mmol of Na_2O_2 act as the metal precursor reducing agents to form ZnO crystal nuclei which grow along the [001] direction. The $C_2H_4(OH)_2$ also acts as a surfactant by absorbing on to the polar surface to prevent ZnO agglomeration along the [001] plane: the cumulative effect being the formation of nanosheets of an approximate size of 800 nm. The $C_2H_4(OH)_2$ acts as a reducing agent for the Ag metal precursor that Ag ions to decorated the ZnO nanosheet.

Microwave solvothermal synthesis within ERTEC microwave applicator [53]

$$\left(CH_3CO_2\right)_2 Zn \cdot 2H_2O + \left(CH_3CO_2\right)_2 Co \cdot 2H_2O \xrightarrow{C_2H_4(OH)_2, H_2O, 190^\circ C} Zn_{1-x}Co_xO + \text{waste products} \quad (4)$$

where $ZnO_{1-x}Co_xO$ represents the general nanostructure at a operating temperature of $T_B = 190^\circ C$ and a autogeneous pressure of 5 bar. The total H_2O contents controls the size of the nanostructure typically less than 1.5% by weight yields a particle size below 28 nm, and 5% by weight yield particle sizes above 53 nm.

Microwave solvothermal synthesis within ERTEC microwave applicator [54]

$$\left(CH_3CO_2\right)_2 Zn \cdot 2H_2O \xrightarrow{C_2H_4(OH)_2, H_2O, 220^\circ C} ZnO + \text{waste products} \quad (5)$$

where ZnO represent the general nanostructure at $T_B = 220^\circ C$ and an autogeneous pressure of 5 bar [55]. As the total H_2O contents increases from 1% to 4% by weight within the reactants a change in morphology is induces, from spheroid to hexagon, as the ZnO(s) grows in size.

5.2. Group V: Pd and Ag

Figure 3 depicts microwave-assisted synthesis energy calculations of five Pd nanostructures reported in publications: Rademacher *et al.* (2022) [56], (Elazab *et al.* (2014) [57], and Elazab, Sadek and El-Idreesy (2018) [58]. In addition fourteen synthesized Ag nanostructures [59]-[71]. The initial feature of these nineteen data points present an elongated cluster over three orders of magnitude along original trend-line. Eighteen of the data points are divided equally, nine between the lower boundary exponent = 0.57 and the original data trend-line, and nine between the original trend-line and the upper boundary exponent = 1. The remaining Ag data point that lies just above the upper boundary exponent = 1 is associated with [38] **Figure 1**. Note how the Pd and Ag data pattern between the upper and lower boundary exponents is markedly different from the ZnO microwave-assisted synthesis data presented in **Figure 2**.

Examining the Pd nanostructure data, there are two applicator-types represented here; a CEM Discover applicator (star) [56], and an unspecified microwave oven rated with a 1 kW CW cavity-magnetron (grey filled circle) [57] [58].

The CEM Discover applicator employs an axial field antenna to create the

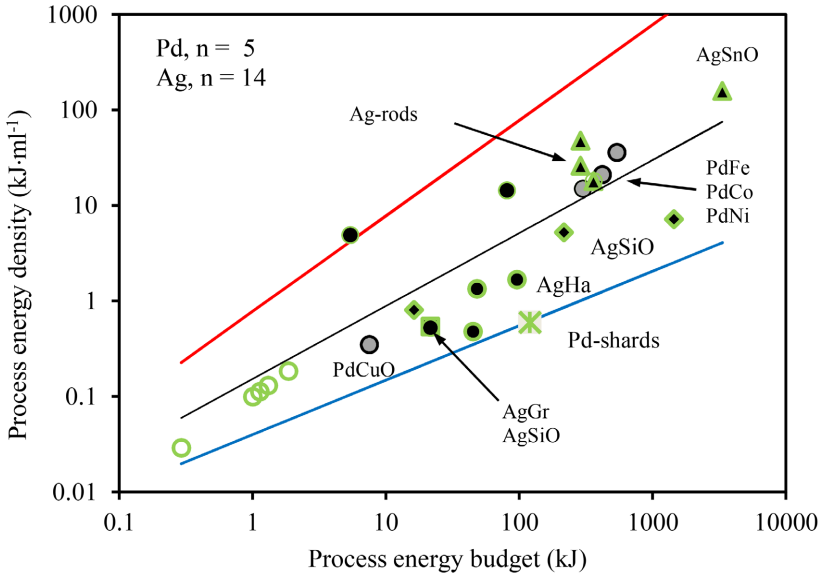

Figure 3. Log-log energy phase-space projection of five Pd (grey and star) and fourteen Ag (black) nanostructures. Star = CEM Discover applicator, circle = Microwave oven applicator, square = TCMC applicator, diamond = ERTEC, and triangle = Digestion applicator. Allometry scaling: red line = exponent 1, blue line = exponent 0.57, and black line = original Database B trend-line with exponent = 0.764.

electromagnetic field processing zone. Both of which are very different electromagnetic field and energy source design ([7] [8], and Öhrngren *et al.* (2012) [72]) to that of the domestic microwave oven. Here the synthesis of Pd shard-like nanostructures have an energy phase-space coordinate of 120 kJ and 0.6 kJ·mol^{-1} and lies at the lower boundary exponent = 0.57 (grey star). The solvent and stabilizing agent propylene carbonate used in the synthesis of the Pd shards, has a low toxicity, and is positioned within the recommended Green Chemistry group.

The unspecified microwave oven employs farmable and toxic hydrazine hydrate as a reducing agent in the synthesis of PdFe, PdCo and PdNi [57], and PdCuO [58]. Together their energy phase-space coordinate are closely aligned (−0.36, + 3.3, +5.5 and +17 kJ·mol^{-1}) to the original data trend-line (grey filled circles with black ring).

An examination of the fourteen Ag dataset reveals they are divided six above and eight below the original data trend-line, with one of the six Ag data points above the upper boundary exponent = 1 [38]. In [38] a one-pot Ag nanostructure synthesis employing $C_{20}H_{24}O_6$ that acts both as reducing and stabilizing reagent within a Samsung CE2877 domestic microwave is reported in this process a cavity-magnetron rated at 850 W is used at 35.3% duty cycle (300 W) for 180 seconds.

The Ag data between the original rend-line and the upper boundary exponent = 1 comprises: one microwave oven and four Digestion applicators. Here, Ahmed *et al.* (2020) [62] used oxalic acid ($C_2H_2O_4$) and cetyltrimethyllammoiumbromide ($C_{19}H_{42}BrN$) to reduce a Samsung microwave oven for synthesis of Ag spherical nanostructures. Alfano *et al.* (2016) [67], and Miglietta *et al.* (2018)

[68]), employed a Anton-Parr Multiwave for synthesis of Ag decorated graphene nanostructures. Liu *et al.* (2005) [69], employs a MARS-5 Digestion applicator for synthesis of Ag nanorods using trisodium citrate ($Na_3C_6H_5O_7$) and Au seeds at 100˚C. Blosi *et al.* (2010) [70] employs a Milstone μSYNTH plus digestion applicator for the synthesis of AgAu core-shells. They use glucose ($C_6H_{12}O_6$) to reduce $HAuCl_4$ in alkaline water. Rai *et al.* (2015) [71] used a MARS-5 Digestion applicator for microwave hydrothermal process (operating temperature = 90˚C, autogeneous pressure not reported) for the synthesis of AgSnO core-shells. Note also that the three digestion applicator synthesis are positioned to the higher end of energy phase-space (>280 kJ).

As regards recommended Green Chemistry, [67] [68] use the $C_2H_6O_2$ in the synthesis of Ag nanostructures, [70] used the eco-friendly $C_6H_{12}O_6$ for the synthesis AgAu core-shells, and [71] uses microwave hydrothermal approach for the synthesis of Ag@SnO_2 core–shells. This recommended Green Chemistry group is annotated in **Figure 3** with a green ring.

Now consider the Ag data points between the original trend-line and the lower boundary exponent = 0.56. In this region there are three microwave ovens and five TCMC applicators synthesizing Ag nanostructures. The microwave oven syntheses are as follows: Saha, Malik and Quresh (2013) [59] Osmium leaf extract of Ag nanostructures. Iqbal, Kadir and Malek (2013) [60] used $C_{19}H_{42}BrN$ in diammonium hydrogen phosphate for substitution of Ca for Ag to form hydroxyapatite (AgHa) nanostructures. Jyothi *et al.* (2020) [61] used *Coleus amboinicus* leaf extract synthesis of Ag nanoparticles.

The TCMC applicators are: TCMC-102 used for carboxymethyl-cellulose sodium ($C_8H_{15}NaO_8$) reduction and capping of Ag nanoparticles (Chen, Wang, Zhangand and Jin (2008) [63]). Karimipour, Shabani and Molaei (2015) [64] used a Shikoku Keisoku SMW 06 fitted with a reflux apparatus for synthesis of Ag nanoparticles. The synthsis used dimethylformamide (C_3H_7NO) as the reducing agent and oleylamine ($C_{18}H_{37}N$) as the capping agent. Ebrahimi, Zakery, Karimipour and Molaei (2016) [65] used the same TCMT applicator for the synthesis of AgTiOs core-shells. Their synthesis used ethanol as the solvent and Polyvinylpyrrolidone-40 ($(C_6H_9NO)_{40}$) as the reducing agent. Karimipour *et al.* (2015) [66]) also used the same TCMT applicator for synthesis of $AgSiO_2$ core-shell nanoparticles. In this synthesis ethanol and C_6H_9NO was used. Again from a recommended Green Chemistry claim, nine publications may be considered [38] [56] [58] [59] [61] [63] [64] [65] [66]. Reference [47] uses NaOH and is part of the problematic group, [60] [62] uses the surfactant.$C_{19}H_{42}BrN$ which in the non-Green Chemistry hazardous group.

5.3. Group VI: Pt and Au

Figure 4 depicts sixteen microwave-assisted synthesized Pt and Au nanostructures mapped in energy phase-space, the upper boundary exponent is kept at a value of 1 and the lower boundary exponent adjusted to 0.7 to intercept the lowest

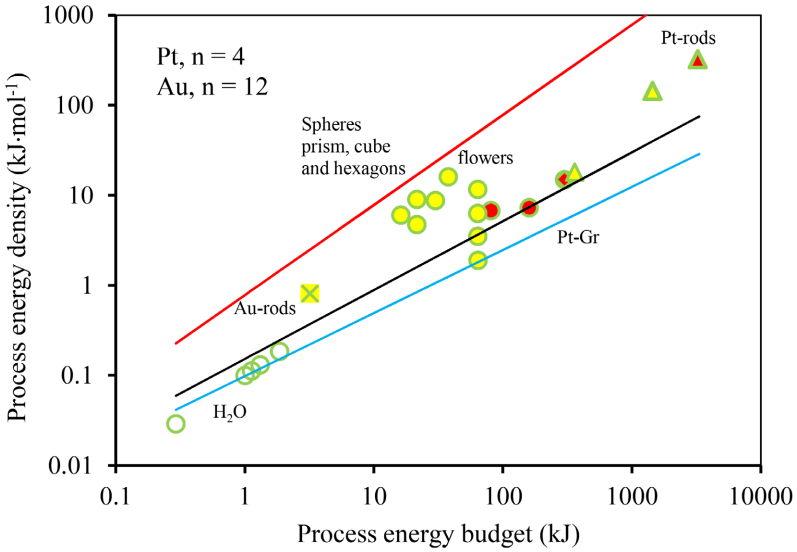

Figure 4. Log-log energy phase-space projection of four Pt (red) and twelve Au (yellow) nanostructures. Yellow star = Discover applicator operating in the continuous-flow mode, Circle = Microwave oven, diamond = ERTEC, and triangle = Digestion applicator. Allometry scaling: red line = exponent 1, blue line = exponent 0.7, and black line = original Database B trend-line with exponent = 0.764.

$kJ \cdot mol^{-1}$ nanostructure data point. The narrowing boundary limit indicates a reduced process energy density bandwidth as compared to the ZnO and the Pd and Ag group.

First consider the four microwave-assisted syntheses of Pt nanostructures (red filled circles and triangle and diamonds). Kundu *et al.* (2011) [73] employs an unspecified microwave oven using ethylene glycol to synthesis Pt-graphene nanostructures (red filled circle with green ring). Pal *et al.* (2014) [74] employs a Samsung CE2877 microwave oven using a mixture $(C_6H_9NO)_n$ and $C_6H_{12}O_6$ to synthesis Pt nanostructurs (red filled circle with green ring). Wojnicki *et al.* (2021) [75] employs an ERTEC applicator working at between 25˚C to 225˚C and autogeneous pressure of 45 to 50 bar (red diamond with green ring). And Li *et al.* (2006) [39] employs a MARS-5 Digestion applicator using the solvothermal technique (T_B = 90˚C, and autogeneous pressure < 200 psi) to produce nanorods (red triangle with green ring). All of these synthesis are located close to the original Database B trend-line with values of: −0.124, +2.324, +3.01 and +25 $kJ \cdot mol^{-1}$, respectively. All four syntheses are placed in the Green Chemistry grouping.

Moving on to the final 12 microwave-assisted synthesized of Au transition metal nanostructures [70] [76]-[84] these are depicted in **Figure 4** using yellow filled circles to depict spheres, and a cross with yellow background to depict nanostructure other than spheres. A green outer ring indicates the use of a Green Chemistry product.

The lowest process budget reported here is the work of Bayazit *et al.* (2016) [76] used the CEM Discover applicator operating in the continuous-flow mode (residence time (τ) typically between 1.5, 0.85, and 0.6 minutes) to anisotropic grow

Au nanorods (star with yellow background). In this synthesis $HAuCl_4{\cdot}4H_2O$ is reduced using $Na_3C_6H_5O_7$ diluted in distilled H_2O at an applied power of 36 W.

Figure 4 also shows that microwave-assisted synthesis of Au nanostructures within domestic microwave ovens that form a cluster within the 16 to 64 kJ process energy budget range. In this cluster Nadagouda and Varma (2007) [77] reports on the use of an inverter circuit [85] within an unspecified Panasonic microwave oven using $C_6H_{12}O_6$, maltose and sucrose ($C_{12}H_{22}O_{11}$) to reduce $HAuCl_4{\cdot}4H_2O$. Here an inverter circuit converts the mains supply frequency (50/60 Hz) to a variable rate of some 20 to 45 kHz and by varying this the cavity-magnetron output power is linearly controlled, in this case 1000 W with a 35 to 45 s illumination time. Yasim, Ramesh and Rajeshkumar (2014) [78] used *hibiscus rosa-sinensis* leaf extract to reduce $HAuCl_4$ within an unspecified domestic microwave oven. The cavity-magnetron conditions used where between 140, 280 and 420 W for a process time of 30, 60, and 90 s to achieve a given nanoparticle size and shape. Bhosale *et al.* (2015) [79] used a LG intellowave™ sensor microwave oven (model unspecified) to synthesis both spherical and flower-like nanoparticles. Their synthesis used the high boiling point (189˚C) lower vapor pressure (0.556 mbar) dimethyl sulfoxide (C_2H_6OS) to reduce $HAuCl_4$. At increasing cavity-magnetron duty cycle, they found that at approximately 30 kJ process energy budget they produced flower-like nanostructures and at an increased energy budget of 64 kJ they produced spherical nanostructures (green circle). Ngo *et al.* (2015) [80] and Ngo *et al.* (2016) [81] used $Na_3C_6H_5O_7$ in H_2O to reduce $HAuCl_4$ within a EMM1908W Electrolux microwave oven. At 210 W and an approximate process energy budget of 64 kJ and process energy density of 3.2 $kJ{\cdot}mol^{-1}$, the process yielded spherical nanoparticles. Shah and Zheng (2019) [82] used (3-mercaptopropyl)trimethoxysilane ($HS(CH_2)_3Si(OCH_3)_3$) plus H_2O to reduce $HAuCl_4$ within a R202ZS Sharp microwave oven. At 800 W the process produced hexagonal Au nanostructures at an approximate process energy budget of 37.8 kJ and process energy density of 16 $kJ{\cdot}mol^{-1}$ (yellow filled circle, black ring). Putri, Pratiwi and Side (2010) [83] used a one-pot synthesis of white bol guava leaf extract in ethanol to reduce $HAuCl_4$ within a NN-SM33HM/W Panasonic microwave oven at 800 W at an approximate process energy budget of 64.3 kJ and process energy density of 1.9 $kJ{\cdot}mol^{-1}$. Blosi *et al.* (2010) [70] used the Milstone μSYNTH digestion applicator that employs two cavity-magnetrons to synthesis Au core bimetallic Au-Ag particles. In this synthesis $HAuCl_4$ was reduced by $C_6H_{12}O_6$ in alkaline H_2O at T_B = 90˚C. The cavity-magnetron applied power was ramped-up and held at a T_B = 80˚C, as determined by software that controls the pulse width modulated power level for 300 s. Finally, Marinoiu *et al.* (2020) [84] used a one-step microwave hydrothermal (T_B = 60˚C to 80˚C, Autogeneous pressure not reported), synthesis of Au nanoparticles supported on a graphene sheet within a MARS-6 digestion applicator (yellow diamond). The synthesis was carried out at a microwave power of 800 W (T_B = 60˚C or 80˚C)

for a process time of 30 minutes.

A Green Chemistry audit of the Au solvents and reagents reveals [70] [76]-[81] [83] [84] can be placed in the recommended Green Chemistry group. Reference [82] with its $HS(CH_2)_3Si(OCH_3)_3$ is in the problematic group.

Figure 5 shows the compilation of the three chemistry groups. The most striking feature here is that the recommended Green Chemistry group ranges from the non-thermal-microwave heating studies in the bottom left to the hydrothermal and solvothemal synthesis in the upper right. For reference note the location of $C_6H_{12}O_6$, maltose and sucrose ($C_{12}H_{22}O_{11}$) [77], *hibiscus rosa-sinensis* leaf extract [78], and white bol guava leaf extract [83]. Here it is worth noting that El-Nagger *et al.* (2016) [86] who used bacterial exopolysaccharide to reduce $HAuCl_4$ to form Au nanostructure is expected to be this region, but insufficient power does not allow the plotting of their data. Secondly the two allometry boundary exponents of 0.66 and 0.87 bracket (capture) the non-Green Chemistry hazardous synthesis which range over two orders of magnitude (10 to 100 kJ). Finally, the problematic group exhibits a tight grouping between 37.5 and 200 kJ with the upper allometry boundary exponent close to 0.94 and the lower allometry exponent close to 0.64, or 0.02 from the non-green chemistry hazardous lower exponent.

6. Summary and Outlook

This work presents a new and novel dual allometry analytical test for the discrimination between three groups of solvent and reagent within a microwave-assisted

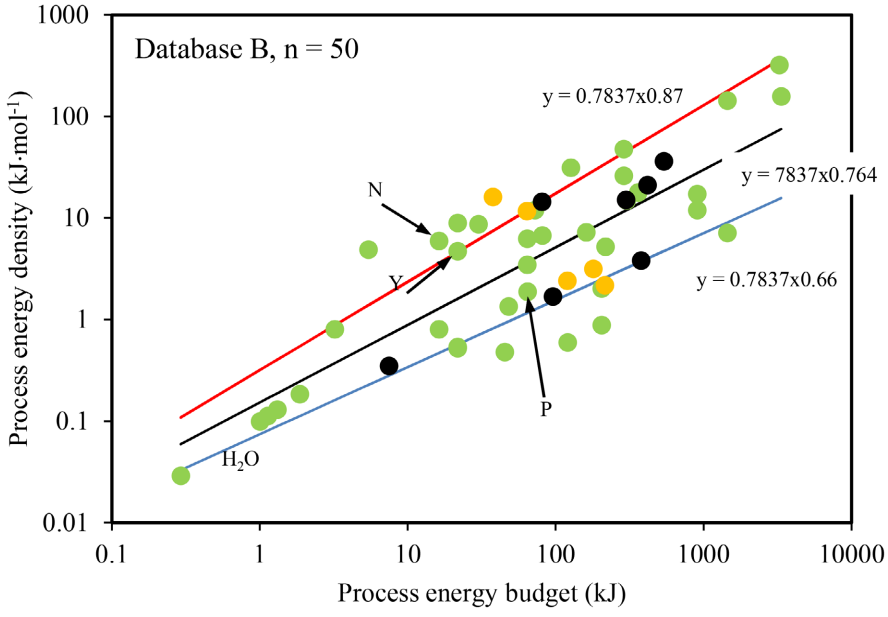

Figure 5. Log-log energy phase-space projection of Green Chemistry (green circles), problematic group (tan circles), non-Green Chemistry hazardous group (black circles). Allometry scaling: red line = exponent 0.87, blue line = exponent 0.66, and black line = original trend-line with exponent = 0.764. The annotated letters N, Y and P correspond to Nadagouda [77] and Yasmim [78] Purti [83].

synthesis power-law signature that is construction from Database B, n = 50. The chemical groups are recommended Green Chemistry, problematic Green Chemistry and non-Green Chemistry hazardous Table 3. The data is presented within energy phase-space projection with dimensions of kJ on the *x*-axes and kJ·mol^{-1} on the *y*-axes. The dual allometry test developed in this work rests on the requirements that the cavity-magnetron power and power on-time, along with the amount of colloidal suspension are measured without error. In addition the *y*-variable be clearly dependent upon the *x*-variable. With fifty different microwave-assisted syntheses spread over five different microwave applicator-types it is inherently unlikely that both of these criteria are met. The choice to use the linear regression best fit trend-line intercept as the allometry intercept must also contribute to the overall error. Given these possible systematic error, discrimination sensitivity to the three chemical groups is achieved. It is shown that the new and novel dual allometry (non-linear) test is suited for the discrimination between three specific chemical groups within the power-law signature. The discrimination being as follows:

1) Recommended Green Chemistry solvent data (for example H_2O and $C_2H_4(OH)_2$) exhibits a broad y-axes distribution within an allometry upper boundary exponent = 1 and lower boundary exponent = 0.5 the intercept of both boundaries are aligned to a power-law signature *y*-axes intercept 0.7837.

2) Problematic Green Chemistry solvent data (for example KOH, NaOH and Na_2O_2) exhibits a narrower distribution on the *y*-axes within an upper exponent = 0.94 and lower exponent = 0.64 where both allometry boundaries are aligned to a power-law signature *y*-axes intercept 0.7837.

3) Non-Green Chemistry hazardous solvent data (for example organic-bromide and flammable/toxic hydrazine hydrate) exhibits a further narrowing of the *y*-axes distribution within the upper exponent = 0.87 and lower exponent = 0.66. Again both allometry boundaries are aligned to a power-law signature *y*-axes intercept 0.7837.

It is also shown that in the *x*-axes direction (process energy budget) the order of magnitude decreases from four orders for recommended Green Chemistry, through two orders for non-Green Chemistry hazardous chemicals and down to one order for problematic Green Chemistry.

This work is in-line with the eleventh principle of Green Chemistry with a focus a non-linear discrimination test between recommended Green Chemistry, problematic Green Chemistry, and Non-Green Chemistry hazardous solvents reagents used in microwave-assisted synthesis of transition metal nanostructures. However, little or no investigation has been performed on the waste byproducts within the cited literature. The tenth principle of Green Chemistry (the breakdown of byproducts to materials that are not harmful to the environment) therefore should be the outlook of this work. It is also thought that the non-linear discrimination test may be applied to other microwave-assisted synthesized metal transition nanostructures.

Conflicts of Interest

The authors declare no conflicts of interest regarding the publication of this paper.

References

[1] Anastas, P. and Eghbali, N. (2010) Green Chemistry: Principles and Practice. *Chemical Society Reviews*, **39**, 301-312. https://doi.org/10.1039/B918763B

[2] Bharadwaj, *et al.* (2021) Green Synthesis of Gold Nanoparticles Using Plant Extracts as Beneficial Prospect for Cancer Theranostics. *Molecules*, **26**, 6389. https://doi.org/10.3390/molecules26216389

[3] Joudeh, N. and Linke, D. (2022) Nanoparticle Classification, Physicochemical Properties, Characterization, and Applications: A Comprehensive Review for Biologists. *Journal of Nanobiotechnology*, **20**, Article No. 262. https://doi.org/10.1186/s12951-022-01477-8

[4] Grewal, A.S., Kumar, K., Redhu, S. and Bhardwaj, S. (2013) Microwave Assisted Synthesis: A Green Synthesis Chemistry Approach. *International Research Journal of Pharmaceutical and Applied Sciences*, **3**, 278-285.

[5] Law, V.J. and Dowling, D.P. (2022) Microwave-Assisted Inactivation of Fomite-Microorganism Systems: Energy Phase-Space Projection. *American Journal Analytical Chemistry*, **13**, 255-276. https://doi.org/10.4236/ajac.2022.137018

[6] Law, V.J. and Dowling, D.P. (2023) Revisiting "Non-Thermal" Batch Microwave Oven Inactivation of Microorganisms. *American Journal of Analytical Chemistry*, **14**, 28-54. https://doi.org/10.4236/ajac.2023.141003

[7] Law, V.J. and Dowling, D.P. (2023) Microwave-Assisted Au and Ag Nanoparticle Synthesis: An Energy Phase-Space Projection Analysis. *American Journal Analytical Chemistry*, **14**, 149-174. https://doi.org/10.4236/ajac.2023.144009

[8] Law, V.J. and Dowling, D.P. (2023) Microwave-Assisted Transition Metal Nanostructure Synthesis: Power-Law Signature Verification. *American Journal Analytical Chemistry*, **14**, 326-349. https://doi.org/10.4236/ajac.2023.148018

[9] Huxley, J.S. and Teissier, G. (1936) Terminology of Relative Growth. *Nature*, **137**, 780-781. https://doi.org/10.1038/137780b0

[10] Huxley, J.S. and Teissier, G. (1936) Terminologie et notation dans la description de la croissance relative. *Comptes rendus des séances de la Société de biologie et de ses filiales*, **121**, 934-937.

[11] Gayon, J. (2000) History of the Concept of Allometry. *American Zoologist*, **40**, 748-758. https://doi.org/10.1093/icb/40.5.748

[12] Galilie, G. (1684) Discorsi e dimostrazioni matematiche intorno á due nuove scienze attinenti alla meccanica & i movimenti locali. Appresso gli Elsevirii.

[13] Thompson, D.W. (1917) On Growth of Forms. Cambridge University Press, Cambridge.

[14] Pézard, A. (1918) Le conditionnement physiologique des caractères sexuels secondaires chez les oiseaux. *Bulletin Biologique de la France et de la Belgique*, **52**, 1-176.

[15] Huxley, J.S. (1924) The Variation in the Width of the Abdomen in Immature Fiddler Crabs Considered in Relation to Its Relative Growth-Rate. *The American Naturalist*, **58**, 468-475. https://doi.org/10.1086/279998

[16] Champy, C. (1924) Sexualite et Hormones. Doin, Paris.

[17] Dong, H., Li, M., Liu, R., Wu, C. and Wu, J. (2017) Allometric Scaling in Scientific

Fields. *Scientometrics*, **112**, 583-594. https://doi.org/10.1007/s11192-017-2333-y

[18] Lamont, B.B., Williams, M.R. and He, T. (2023) Relative Growth Rate (RGR) and Other Confounded Variables: Mathematical Problems and Biological Solutions. *Annals of Botany*, **131**, 555-567. https://doi.org/10.1093/aob/mcad031

[19] Kleiber, M. (1932) Body Size and Metabolism. *Hilgardia*, **6**, 315-353. https://doi.org/10.3733/hilg.v06n11p315

[20] Kleiber, M. (1947) Body Size and Metabolic Rate. *Physiological Review*, **27**, 511-541. https://doi.org/10.1152/physrev.1947.27.4.511

[21] Niklas, K.J. and Kutschera, U. (2015) Kleiber's Law: How the Fire of Life Ignited Debate, Fueled Theory, and Neglected Plants as Model Organisms. *Plant Signaling & Behavior*, **10**, e1036216. https://doi.org/10.1080/15592324.2015.1036216

[22] Rue, A.R.P. (2002) Biological Scaling and Physics. *Journal of Biosciences*, **27**, 475-478. https://doi.org/10.1007/BF02705043

[23] Stumpf, M.P.H. and Porter, M.A. (2012) Critical Truths about Power Laws. *Science*, **355**, 665-666. https://doi.org/10.1126/science.1216142

[24] Andriani, P. and McKelvey, B. (2009) From Gaussian to Paretian Thinking: Causes and Implications of Power Laws in Organizations. *Perspective Organization Science*, **20**, 1053-1071. https://doi.org/10.1287/orsc.1090.0481

[25] Roman, S. and Bertolotti, F. (2020) A Master Equation for Power Laws. *Royal Society Open Science*, **9**, Article ID: 220531. https://doi.org/10.1098/rsos.220531

[26] West, G.B., Brown, J.H. and Enquist, B. (1997) A General Model for the Origin of Allometric Scaling Laws in Biology. *Science*, **276**, 122-126. https://doi.org/10.1126/science.276.5309.122

[27] West, G.B., Brown, J.H. and Enquist, B.J. (1999) A General Model for the Structure and Allometry of Plant Vascular Systems. *Nature*, **399**, 664-667. https://doi.org/10.1038/23251

[28] Lindstedt, S.L. (1981) Body Size, Physiological Time, and Longevity of Homeothermic Animals. *The Quarterly Review of Biology*, **56**, 1-16. https://doi.org/10.1086/412080

[29] Agutter, P.S. and Tuszynski, J.A. (2011) Analytic Theories of Allometric Scaling. *The Journal of Experimental Biology*, **214**, 1055-1062. https://doi.org/10.1242/jeb.054502

[30] Gillooly, J.F., Brown, J.H., West, G.B., Savage, V.M. and Charnov, E.L. (2001) Effect of Size and Temperature on Metabolic Rate. *Science*, **293**, 2248-2251. https://doi.org/10.1126/science.1061967

[31] Downs, C.J., Hayes, J.P. and Tracy, C.T. (2008) Scaling Metabolic Rate with Body Mass and Inverse Temperature: A Test of the Arrhenius Fractal Supply Model. *Functional Ecology*, **22**, 239-244. https://doi.org/10.1111/j.1365-2435.2007.01371.x

[32] Dedrick, R.L., Bischolt, K.B. and Zaharko, D.Z. (1970) Interspecies Correlation of Plasma Concentration History of Methotrexate (NSC-740). *Cancer Chemotherapy Reports*, *Part* 1, **54**, 95-101.

[33] Boxenbaum, H. (1981) Interspecies Scaling, Allometry, Physiological Time, and the Ground Plan of Pharmacokinetics. *Journal of Pharmacokinetics and Biopharmaceutics*, **10**, 201-227. https://doi.org/10.1007/BF01062336

[34] Boxenham, H. and Fertig, J.B. (1984) Scaling of Antipyrine Intrinsic Clearance of Unbound Drug in 15 Mammalian Species. *European Journal of Drug Metabolism and Pharmacokinetics*, **9**, 177-183. https://doi.org/10.1007/BF03189622

[35] Gilibili, R.R., Bhamidipati, R.K., Mullangi, R. and Srinivas, N.R. (2015) Retrospec-

tive and Prospective Human Intravenous and Oral Pharmacokinetic Projection of Dipeptidyl Peptidase-IV Inhibitors Using Simple Allometric Principles-Case Studies of ABT-279, ABT-341, Alogliptin, Carmegliptin, Sitagliptin and Vildagliptin. *Journal of Pharmacy & Pharmaceutical Sciences*, **18**, 434-447. https://doi.org/10.18433/J3TK55

[36] Andresen, B., Shiner, J.S. and Uehlinger, D.E. (2002) Allometric Scaling and Maximum Efficiency in Physiological Eigen Time. *Proceedings of the National Academy of Sciences*, **99**, 5822-5824. https://doi.org/10.1073/pnas.082633699

[37] Liu, S., Maljovec, D., Wang, B., Bremer, P.T. and Pascucci, V. (2017) Visualizing High-Dimensional Data: Advances in the Past Decade. *IEEE Transaction on Visualization and Computer Graphs*, **23**, 1249-1268. https://doi.org/10.1109/TVCG.2016.2640960

[38] Pal, J., Deb, M.K. and Deshmukh, D.K. (2014) Microwave-Assisted Synthesis of Silver Nanoparticles Using Benzo-18-crown-6 as Reducing and Stabilizing Agent. *Applied Nanoscience*, **4**, 507-510. https://doi.org/10.1007/s13204-013-0229-6

[39] Li, D. and Komarneni, S. (2006) Synthesis of Pt Nanoparticles and Nanorods by Microwave-Assisted Solvothermal Technique. *Zeitschrift fuer Naturforschung. B*, **61**, 1566-1572. https://doi.org/10.1515/znb-2006-1214

[40] Law, V.J. and Dowling, D.P. (2021) Microwave Generated Steam Decontamination of Respirators: Dielectric Considerations. *Global Journal of Research in Engineering & Computer Sciences*, **1**, 6-21.

[41] Rana, K.K. and Rana, S. (2014) Microwave Reactors: A Brief Review on Its Fundamental Aspects and Applications. *Open Access Library Journal*, **1**, e686. https://doi.org/10.4236/oalib.1100686

[42] Patil, N.G., Rebrov, E.V., Eranen, K., Benaskar, F., Meuldijk, J., Mikkola, J.P., Hessel, V., Hulshof, L.A., Murzin, D.Y. and Schouten, J.C. (2012) Effect of the Load Size on the Efficiency of Microwave Heating under Stop Flow and Continuous Flow Conditions. *Journal of Microwave Power and Electromagnetic Energy*, **46**, 83-92. https://doi.org/10.1080/08327823.2012.11689827

[43] Welton, T. (2015) Solvents and Sustainable Chemistry. *Proceedings of the Royal Society A*, **471**, Article ID: 20150502. https://doi.org/10.1098/rspa.2015.0502

[44] Cao, J. and Wang, J. (2004) Microwave-Assisted Synthesis of Flower-Like ZnO Nanosheet Aggregates in a Room-Temperature Ionic Liquid. *Chemistry Letters*, **33**, 1332-1333. https://doi.org/10.1246/cl.2004.1332

[45] Krishnapriya, R., Praneetha, S. and Murugan, A.V. (2016) Investigation of the Effect of Reaction Parameters on the Microwave-Assisted Hydrothermal Synthesis of Hierarchical Jasmine-Flower-Like ZnO Nanostructures for Dye-Sensitized Solar Cells. *New Journal of Chemistry*, **40**, 5080-5089. https://doi.org/10.1039/C6NJ00457A

[46] Cao, Y., Liu, B., Huang, R., Xia, Z. and Flash, S.G. (2011) synthesis of Flower-Like ZnO Nanostructures by Microwave-Induced Combustion Process. *Materials Letters*, **65**, 160-163. https://doi.org/10.1016/j.matlet.2010.09.072

[47] Li, H., Liu, E., Chan, F.Y.E., Lu, Z. and Chen, R. (2011) Fabrication of Ordered Flower-Like ZnO Nanostructures by a Microwave and Ultrasonic Combined Technique and Their Enhanced Photocatalytic Activity. *Materials Letters*, **65**, 3440-3443. https://doi.org/10.1016/j.matlet.2011.07.049

[48] Hasanpoor, M., Aliofkhazraei, M. and Delavari, H. (2015) Microwave-Assisted Synthesis of Zinc Oxide Nanoparticles. *Procedia Materials Science*, **11**, 320-325. https://doi.org/10.1016/j.mspro.2015.11.101

[49] Liu, H., Liu, H., Yang, J., Zhai, H., Liu, X. and Jia, H. (2019) Microwave-Assisted

One-Pot Synthesis of Ag Decorated Flower-Like ZnO Composites Photocatalysts for Dye Degradation and NO Removal. *Ceramics International*, **45**, 20133-20140. https://doi.org/10.1016/j.ceramint.2019.06.279

[50] Aljaafari, A., Ahmed, F., Awada, C. and Shaalan, N.M. (2020) Flower-Like ZnO Nanorods Synthesized by Microwave-Assisted One-Pot Method for Detecting Reducing Gases: Structural Properties and Sensing Reversibility. *Frontiers in Chemistry*, **8**, Article No. 456. https://doi.org/10.3389/fchem.2020.00456

[51] Cai, Y. and Hung, J. (2023) Preparation and Photocatalysis Characteristics of Flower-Like ZnO by Microwave Method. *Journal of Physics*: *Conference Series*, **2437**, Article ID: 012039. https://doi.org/10.1088/1742-6596/2437/1/012039

[52] Li, X., Wang, C., Zhou, X., Liu, J., Sun, P. and Lu, G. (2014) Gas Sensing Properties of Flower-Like ZnO Prepared by a Microwave-Assisted Technique. *Royal Society of Chemistry Advances*, **4**, 47319-47324. https://doi.org/10.1039/C4RA07425D

[53] Wojnarowicz, J., Chudoba, T., Gierlotka, S., Sobczak, K. and Lojkowski, W. (2018) Size Control of Cobalt-Doped ZnO Nanoparticles Obtained in Microwave Solvothermal Synthesis. *Crystals*, **8**, Article No. 179. https://doi.org/10.3390/cryst8040179

[54] Wojnarowicz, J., Opalinska, A., Chudoba, T., Gierlotka, S., Mukhovskyi, R., Pietrzykowska, E., Sobczak, K. and Lojkowski, W. (2016) Effect of Water Content in Ethylene Glycol Solvent on the Size of ZnO Nanoparticles Prepared Using Microwave Solvothermal Synthesis. *Journal of Nanomaterials*, **2016**, Article ID: 2789871. https://doi.org/10.1155/2016/2789871

[55] Wojnarowicz, J. (2023) Institute of High Pressure Physics, Polish Academy of Sciences, Sokolowska 29/37, 01-142 Warsaw, Poland. Private Communication regarding Operating Pressure of ERTEC Microwave Applicator Used in Reference [53].

[56] Rademacher, L., Yen Beglau, T.H., Heinen, T., Barthel and Janiak, C. (2020) Microwave-Assisted Synthesis of Iridium Oxide and Palladium Nanoparticles Supported on a Nitrogen-Rich Covalent Triazine Framework as Superior Electrocatalysts for the Hydrogen Evolution and Oxygen Reduction Reaction. *Frontiers of Chemistry*, **10**, Article No. 94526. https://doi.org/10.3389/fchem.2022.945261

[57] Elazab, H.A., Moussa, S., Gupton, B.F. and El-Shall, M.S. (2014) Microwave-Assisted Synthesis of Pd Nanoparticles Supported on Fe_3O_4, Co_3O_4, and $Ni(OH)_2$ Nanoplates and Catalysis Application for CO Oxidation. *Journal of Nanoparticle Research*, **16**, Article No. 2477. https://doi.org/10.1007/s11051-014-2477-0

[58] Elazab, H.A., Sadek, M.A. and El-Idreesy, T.T. (2018) Microwave-Assisted Synthesis of Palladium Nanoparticles Supported on Copper Oxide in Aqueous Medium as an Efficient Catalyst for Suzuki Cross-Coupling Reaction. *Adsorption Science & Technology*, **36**, 135-1365. https://doi.org/10.1177/0263617418771777

[59] Saha, S., Malik, M.M. and Qureshi, M.S. (2013) Microwave Synthesis of Silver Nano Particles. *Nano Hybrids*, **4**, 99-112. https://doi.org/10.4028/www.scientific.net/NH.4.99

[60] Iqbal, N., Kadir, M.R.A., Malek, N.A.N.N., Mahmood, N.H.B., Murali, M.R. and Kamarul, T. (2013) Characterization and Antibacterial Properties of Stable Silver Substituted Hydroxyapatite Nanoparticles Synthesized through Surfactant Assisted Microwave Process. *Materials Research. Bulletin*, **48**, 3172-3177. https://doi.org/10.1016/j.materresbull.2013.04.068

[61] Jyothi, D., Cherriyan, S.P., Ahmed, S.R.R., Priya, S. and James, J.P. (2020) Microwave-Assisted Green Synthesis of Silver Nanoparticles Using Coleus Amboinicus Leaf Extract. *International Journal of Applied Pharmaceutics*, **12**, 56-61. https://doi.org/10.22159/ijap.2020v12i3.37121

[62] Ahmed, F., AlOmar, S.Y., Albalawi, F., Arshi, N., Dwivedi, S., Kumar, S., Shaalan, N.M. and Ahmad, N. (2021) Microwave Mediated Fast Synthesis of Silver Nanoparticles and Investigation of Their Antibacterial Activities for Gram-Positive and Gram-Negative Microorganisms. *Crystals*, **11**, Article No. 666. https://doi.org/10.3390/cryst11060666

[63] Chen, J., Wang, J., Zhang, X. and Jin, Y. (2008) Microwave-Assisted Green Synthesis of Silver Nanoparticles by Carboxymethyl Cellulose Sodium and Silver Nitrate. *Materials Chemistry and Physics*, **108**, 421-424. https://doi.org/10.1016/j.matchemphys.2007.10.019

[64] Karimipour, M., Shabani, E. and Molaei, M. (2015) Microwave Synthesis of Oleylamine-Capped Ag Nanoparticles in Aqueous Solution. *Materials Science*, **21**, 182-186. https://doi.org/10.5755/j01.ms.21.2.6480

[65] Ebrahimi, M., Zakery, A., Karimipour, M. and Molaei, M. (2016) Nonlinear Optical Properties and Optical Limiting Measurements of Graphene Oxide Ag@TiO_2 Compounds. *Optical Materials*, **57**, 146-152. https://doi.org/10.1016/j.optmat.2016.04.039

[66] Karimipour, M., Mostoufirad, S., Molaei, M., Nikabadi, H.R. and Nesheli, A.G. (2016) Free Reducing Agent, One Pot, and Two Steps Synthesis of Ag@SiO_2 Core-Shells Using Microwave Irradiation. *Journal of Nano- and Electronic Physics*, **8**, Article No. 03020. https://doi.org/10.21272/jnep.8(3).03020

[67] Alfano, B., Polichetti, T., Mauriello, M., Miglietta, M.L., Ricciardella, F., Massera, E. and Francia, G.D. (2016) Modulating the Sensing Properties of Graphene through an Eco-Friendly Metal-Decoration Process. *Sensors and Actuators B*: *Chemical*, **222**, 1032-1042. https://doi.org/10.1016/j.snb.2015.09.008

[68] Miglietta, M.L., Alfano, B., Polichetti, T., Massera, E., Schiattarella, C. and Francia, G.D. (2018) Effective Tuning of Silver Decorated Graphene Sensing Properties by Adjusting the Ag NPs Coverage Density. *Sensors*: *Proceedings of the* 3*rd National Conference on Sensors*, Rome, 23-25 February 2016, 82-89.

[69] Liu, F.K., Huang, P.W., Chang, Y.C., Ko, C.J., Ko, F.H. and Chu, T.C. (2005) Formation of Silver Nanorods by Microwave Heating in the Presence of Gold Seeds. *Journal of Crystal Growth*, **273**, 439-445. https://doi.org/10.1016/j.jcrysgro.2004.09.043

[70] Blosi, M., Albonetti, S., Gatti, F., Dondi, M., Migliori, A., Ortolani, L., Morandi, V. and Baldi, G. (2010) Au, Ag and Au-Ag Nanoparticles: Microwave-Assisted Synthesis in Water and Applications in Ceramic and Catalysis. *Nanotech*, **1**, 352-355.

[71] Rai, P., Majhi, S.M., Yu, Y.T. and Lee, J.H. (2015) Synthesis of Plasmonic Ag@SnO_2 Core-Shell Nanoreactors for Xylene Detection. *Royal Society of Chemistry*, **5**, 17653-17659. https://doi.org/10.1039/C4RA13971B

[72] Ohrngren, P., Fardost, A., Russo, F., Schanche, J.S., Fagrell, M. and Larhed, M. (2012) Evaluation of a Nonresonant Microwave Applicator for Continuous-Flow Chemistry Applications. *American Chemical Society*, **16**, 1053-1063. https://doi.org/10.1021/op300003b

[73] Kundu, P., Nethravathi, C., Deshpande, P.A., Rajamathi, M., Madras, G. and Ravishankar, N. (2011) Ultrafast Microwave-Assisted Route to Surfactant-Free Ultrafine Pt Nanoparticles on Graphene: Synergistic Co-Reduction Mechanism and High Catalytic Activity. *Chemistry of Materials*, **23**, 2772-2780. https://doi.org/10.1021/cm200329a

[74] Pal, J., Deb, M.K., Deshmukh, D.K. and Sen, B.K. (2014) Microwave-Assisted Synthesis of Platinum Nanoparticles and Their Catalytic Degradation of Methyl Violet in Aqueous Solution. *Applied Nanoscience*, **4**, 61-65.

https://doi.org/10.1007/s13204-012-0170-0

[75] Wojnicki, M., Luty-Błocho, M., Kwolek, P., Gajewska, M., Socha, R.P., Pędzich, Z., Csapó, E. and Hessel, V. (2021) The Influence of Dielectric Permittivity of Water on the Shape of PtNPs Synthesized in High-Pressure High-Temperature Microwave Reactor. *Scientific Reports*, **11**, Article No. 4851. https://doi.org/10.1038/s41598-021-84388-2

[76] Bayazit, M.K., Yue, J., Cao, E., Gavriilidis, A. and Tang, J. (2016) Controllable Synthesis of Gold Nanoparticles in Aqueous Solution by Microwave Assisted Flow Chemistry. *ACS Sustainable Chemistry & Engineering*, **4**, 6435-6442. https://doi.org/10.1021/acssuschemeng.6b01149

[77] Nadagouda, M.N. and Varma, R.S. (2007) Microwave-Assisted Shape-Controlled Bulk Synthesis of Noble Nanocrystals and Their Catalytic Properties. *Crystal Growth & Design*, **8**, 291-295.

[78] Yasmin, A., Ramesh, K. and Rajeshkumar, S. (2014) Optimization and Stabilization of Gold Nanoparticles by Using Herbal Plant Extract with Microwave Heating. *Nano Convergence*, **1**, Article No. 12. https://doi.org/10.1186/s40580-014-0012-8

[79] Bhosale, M.A., Chenna, D.R., Ahire, J.P. and Bhanage, B.M. (2015) Morphological Study of Microwave-Assisted Facile Synthesis of Gold Nanoflowers/Nanoparticles in Aqueous Medium and Their Catalytic Application for Reduction of p-Nitrophenol to p-Aminophenol. *Royal Society of Chemistry Advances*, **5**, 52817-52823. https://doi.org/10.1039/C5RA05731K

[80] Ngo, V.K.T., Nguyen, H.P.U., Huynh, T.P., Tran, N.N.P., Lam, Q.V. and Huynh, T.D. (2015) Preparation of Gold Nanoparticles by Microwave Heating and Application of Spectroscopy to Study Conjugate of Gold Nanoparticles with Antibody *E. coli* O157:H7. *Advances in Natural Sciences*: *Nanoscience and Nanotechnology*, **6**, Article ID: 035015. https://doi.org/10.1088/2043-6262/6/3/035015

[81] Ngo, V.K.T., Nguyen, H.P.U., Huynh, T.P. and Lam, Q.V. (2016) A Low Cost Technique for Synthesis of Gold Nanoparticles Using Microwave Heating and Its Application in Signal Amplification for Detecting *Escherichia coli* O157:H7 Bacteria. *Advances in Natural Sciences*: *Nanoscience and Nanotechnology*, **7**, Article ID: 035016. https://doi.org/10.1088/2043-6262/7/3/035016

[82] Shah, K.W. and Zheng, L. (2019) Microwave-Assisted Synthesis of Hexagonal Gold Nanoparticles Reduced by Organosilane (3-Mercaptopropyl)trimethoxysilane. *Materials*, **12**, Article No. 11. https://doi.org/10.3390/ma12101680

[83] Putri, S.E., Pratiwi, D.E. and Side, S. (2021) The Effect of Microwave Irradiation on Synthesis of Gold Nanoparticles Using Ethanol Extract of White Bol Guava Leaves. *Journal of Physics*: *Conference Series*, **1752**, Article ID: 012058. https://doi.org/10.1088/1742-6596/1752/1/012058

[84] Marinoiu, A., Andrei, R., Vagner, I., Niculescu, V., Bucra, F., Constantinescu, M. and Carcadea, E. (2020) One Step Synthesis of Au Nanoparticles Supported on Graphene Oxide Using an Eco-Friendly Microwave-Assisted Process. *Materials Science*, **26**, 249-254. https://doi.org/10.5755/j01.ms.26.3.21857

[85] Min, G.I., Han, S.J. and Shin, D.M. (2005) Inverter Circuit of Microwave Oven. US Patent 6,936,803 B2. (Issued August 30, 2005).

[86] El-Naggar, M.E., Shaheen, T.I., Fouda, M.M.G. and Hebeish, A.A. (2016) Eco-Friendly Microwave-Assisted Green and Rapid Synthesis of Well-Stabilized Gold and Core-Shell Silver-Gold Nanoparticles. *Carbohydrate Polymers*, **20**, 1128-1136. https://doi.org/10.1016/j.carbpol.2015.10.003